

# Basis-constrained Bayesian Markov-chain Monte Carlo difference inversion for geoelectrical monitoring of hydrogeologic processes

Erasmus Kofi Oware<sup>1</sup>, James Irving<sup>2</sup>, and Thomas Hermans<sup>3</sup>

## ABSTRACT

Bayesian Markov-chain Monte Carlo (McMC) techniques are increasingly being used in geophysical estimation of hydrogeologic processes due to their ability to produce multiple estimates that enable comprehensive assessment of uncertainty. Standard McMC sampling methods can, however, become computationally intractable for spatially distributed, high-dimensional problems. We have developed a novel basis-constrained Bayesian McMC difference inversion framework for time-lapse geophysical imaging. The strategy parameterizes the Bayesian inversion model space in terms of sparse, hydrologic-process-tuned bases, leading to dimensionality reduction while accounting for the physics of

the target hydrologic process. We evaluate the algorithm on cross-borehole electrical resistivity tomography (ERT) field data acquired during a heat-tracer experiment. We validate the ERT-estimated temperatures with direct temperature measurements at two locations on the ERT plane. We also perform the inversions using the conventional smoothness-constrained inversion (SCI). Our approach estimates the heat plumes without excessive smoothing in contrast with the SCI thermograms. We capture most of the validation temperatures within the 90% confidence interval of the mean. Accounting for the physics of the target process allows the detection of small temperature changes that are undetectable by the SCI. Performing the inversion in the reduced-dimensional model space results in significant gains in computational cost.

## INTRODUCTION

Understanding subsurface processes is critical to the design and efficient management of groundwater and energy resources. Although traditional well-based sampling methods provide valuable insights into subsurface processes (e.g., LeBlanc et al., 1991), they are expensive and provide limited spatiotemporal information. The use of geophysical methods to investigate spatially continuous hydrogeologic processes is well-documented (e.g., Singha et al., 2015). The inversion of geophysical data is, however, nontrivial due to limited noisy data (ill-posedness) and solution nonuniqueness (Menke, 1984). Typically, regularization is required to stabilize the problem and obtain a unique result (Tikhonov and Arsenin, 1977).

Traditional regularization constraints impose smoothness and/or force the solution toward some reference model (Menke, 1984) without accounting for our prior understanding of the physics of the target hydrologic process. In solute plume moments' inference from tomograms, Day-Lewis et al. (2007) show that the choice of

regularization strongly influences the solution, often producing smoothed-out plumes with mass under-estimation. The coupled (Hinnell et al., 2010) and basis-constrained (Oware et al., 2013) inversion frameworks were developed to address the lack of physics-based prior in the traditional regularization constraints.

Although deterministic methods provide simple and computationally efficient inversion frameworks, stochastic inversion (SI) techniques enable comprehensive interpretation of the estimates (Tarantola, 2005) with the capacity to estimate geologically realistic features (e.g., Oware, 2016). Bayesian Markov-chain Monte Carlo (McMC) is a commonly used SI strategy in hydrogeophysics (e.g., Irving and Singha, 2010). Standard McMC sampling methods can, however, become computationally expensive when working with spatially distributed (high-dimensional) geophysical parameter fields. In such cases, performing McMC in a reduced-dimensional space may help to render the stochastic inverse problem computationally tractable (e.g., Ruggeri et al., 2015). Multivariate statistical tools for dimensionality reduction (e.g., proper orthogonal decom-

Manuscript received by the Editor 6 September 2018; revised manuscript received 2 December 2018; published ahead of production 19 March 2019; published online 3 May 2019.

<sup>1</sup>SUNY at Buffalo, Department of Earth Sciences, Buffalo, New York, USA. E-mail: erasmuso@buffalo.edu (corresponding author).

<sup>2</sup>University of Lausanne, Institute of Earth Sciences, Lausanne, Switzerland. E-mail: james.irving@unil.ch.

<sup>3</sup>Ghent University, Department of Geology, Ghent, Belgium. E-mail: thomas.hermans@UGent.be.

© 2019 Society of Exploration Geophysicists. All rights reserved.

position (POD) or singular value decomposition (SVD), eigenvector, and wavelet transformations) typically find an orthogonal set of basis vectors that capture the maximum amount of variability in a training data set, thereby enabling a sparse representation of the chosen system.

Hermans et al. (2016) apply a prediction-focused approach (PFA) (Satija and Caers, 2015) for direct stochastic prediction of hydrogeologic parameters without the need for classic inversion. Although PFA circumvents classic inversion of the data, it relies on trained statistical relationship for prediction without the process of actually fitting the data, which limits its ability to reconstruct features that are not well-represented in the training data. Furthermore, the dimensionality reduction can also be achieved via frequency-amplitude-based bases and orthogonal moments. Lochbuhler et al. (2014) successfully apply discrete cosine transform (DCT) parameterization of the model space for probabilistic electrical resistivity characterization of a lab-scale CO<sub>2</sub> injection experiment. We contend that, unlike process-tuned, nonparametric bases, the parametric DCT bases are fixed, which will limit their ability to reconstruct complex plume morphologies. In a synthetic example, Laloy et al. (2012) successfully perform MCMC in the lower dimensional model space related to Legendre moments. In an attempt to produce realistic plume morphologies with mass conservation, they predefine mass and morphological features, which imposed hard constraints that are typically unknown a priori in real-world data. We present a novel basis-constrained Bayesian MCMC (BcB-McMC) difference inversion framework to improve monitoring of hydrogeologic processes. The method constrains the classical Bayesian inversion scheme with hydrologic-process-tuned, nonparametric bases to account for the physics of the target process. The key contributions of the algorithm are that (1) it allows the incorporation of site-specific, hydrologic-process-tuned nonparametric bases, (2) it parameterizes the Bayesian inversion problem in the reduced-dimensional space, and (3) it does not require prior specifications of mass and plume geometric features. It also provides a simple, general framework to incorporate bases constructed from different methods for finding orthogonal bases. We illustrate the performance of the algorithm on a field-scale geoelectrical data acquired during a heat-tracer experiment.

In spite of the numerous advantages of SI, most of the SI strategies in hydrogeophysics have focused on characterization of aquifer heterogeneities (e.g., Linde et al., 2006; Oware, 2016) with limited techniques addressing the important subject of subsurface solute-plume characterization. This contribution provides a new perspective on SI frameworks for geophysical monitoring of subsurface solute-plumes.

## BASIS-CONSTRAINED BAYESIAN McMC DIFFERENCE INVERSION

Oware et al. (2013) present the basis-constrained inversion, wherein a vector of the target model  $\sigma$  is expressed as a linear combination of its basis vectors  $\mathbf{B}$  and coefficients  $\mathbf{c}$

$$\sigma = \mathbf{B}\mathbf{c}. \quad (1)$$

They implement equation 1 in a classical Tikhonov deterministic inversion scheme to infer the optimal set of coefficients from geophysical measurements. Here, we formulate a Bayesian MCMC version of the basis-constrained inversion as

$$\mathbf{c}_{\text{post}} = \mathbf{c}_{\text{prior}} L(\sigma | \mathbf{d}_{\text{obs}}) = \mathbf{c}_{\text{prior}} L(\mathbf{B}, \mathbf{c} | \mathbf{d}_{\text{obs}}), \quad (2)$$

where  $\mathbf{c}_{\text{post}}$  and  $\mathbf{c}_{\text{prior}}$  are the posterior and prior coefficients, respectively, and  $L(\bullet)$  is the likelihood function, which evaluates the probability of a proposed model given the observed data. We implement equation 2 as a difference inversion framework (LaBrecque and Yang, 2001). In addition to its rapid convergence, difference inversion is intuitively appealing for monitoring hydrogeologic processes due to its ability to detect small changes, eliminate systematic errors, and reduce inversion artifacts. Hence, adopting the Bayesian view of regularization (e.g., MacKay, 1992) for computational stability, we compute the regularized likelihood as

$$L(\mathbf{B}, \mathbf{c}, \mathbf{W}_d, \beta | \mathbf{d}_{\text{obs}}) = \exp \left[ -\frac{1}{2} (\mathbf{e}^T * \mathbf{W}_d * \mathbf{e} + \beta \mathbf{c}^T * \mathbf{W}_c * \mathbf{c}) \right], \quad (3)$$

where the data misfit expressed in terms of a difference is  $\mathbf{e} = [\mathbf{d}_t - \mathbf{d}_0] - [f(\mathbf{B}\mathbf{c}) - f(\sigma_0)]$ , with  $\mathbf{d}_t$  and  $\mathbf{d}_0$  representing data at the time-step of interest and background, respectively. The terms  $f(\sigma_0)$  and  $f(\mathbf{B}\mathbf{c})$  are, respectively, the forward simulations from the classical inversion ( $\sigma_0$ ) of the background data and the proposed model. The term  $\mathbf{W}_d$  is the data-weight matrix,  $\beta$ , arbitrarily set to 1e-6 here, is a fitting parameter. The value for  $\beta$  can also be determined using the L-curve approach (Hansen and O'Leary, 1993). The term  $\mathbf{W}_c$  denotes the coefficient regularization operator, which contains the inverse of the fractional contributions of the singular values of the basis vectors, to impose prior structural constraints on  $\mathbf{c}$  (e.g., Oware and Moysey, 2014).

To summarize the workflow of the BcB-McMC, first, we perform Monte Carlo simulations of training images (TIs) tuned to the physics of the target hydrologic process to capture, for instance, multiple rates of advection and multiple scales of dispersion and complexities in the plume morphologies. We pull all the simulated time lapse hydrologic models together into a single robust library of TIs. Second, we construct orthogonal bases  $\mathbf{B}$  from the TIs. Third, to obtain prior distributions of the coefficients  $\mathbf{c}_{\text{prior}}$ , we project the TIs onto  $\mathbf{B}$ . Fourth, we propose coefficients from  $\mathbf{c}_{\text{prior}}$ . We accept or reject the proposed coefficients based on the classic Metropolis-Hastings acceptance rule (Metropolis et al., 1953; Hastings, 1970). The posterior coefficients are then mapped onto the bases to obtain multiple realizations of the target.

## APPLICATION TO FIELD DATA

### Heat-tracer and ERT Experiments

We demonstrate the performance of the algorithm on a field-scale heat-tracer experiment conducted in an alluvial aquifer and monitored with cross-borehole electrical resistivity tomography (XBh-ERT). Details of the heat-tracer and XBh-ERT experimental designs are outlined in Hermans et al. (2015). To summarize, water was continuously pumped to induce groundwater flow toward the pumping well. Hot water was then injected continuously in an injection well for 24 h. Changes in electrical conductivity were monitored in an XBh-ERT panel perpendicular to the flow direction. Here, we focus on the inversion of the first six time-lapse profiles (e.g., Hermans et al., 2018) acquired at 6, 12, 18, 21.5, 25, and 30 h after the commencement of the heat injection. After data filtering (Hermans et al., 2018), all the inversions involved only 410 quadrupoles for each time

step. During the experiments, direct temperatures were monitored in two piezometers, pz14 and pz15 located along the ERT plane.

## Inversion procedure

The first step in the inversion involves Monte Carlo simulations of TIs tuned to the physics of the presupposed heat-tracer experiment. We used the same 3000 (500 models x 6 time steps) TIs used by Hermans et al. (2018). The key in the TI simulations is to generate site-specific, physically realistic plume morphologies with uncertainties in the underlying hydrogeologic properties consistent with prior knowledge of the site. Here, we considered Gaussian hydraulic conductivity  $K$  fields with uncertainties in the mean  $K$  and variance, anisotropy, and orientation. The heat transport assumes advection and dispersion and retardation due to the heat capacity of the solids. We refer to Hermans et al. (2018) for more details about the generation of the TIs. We then constructed the basis vectors from the TIs (log of electrical resistivity) using POD. Although there are various methods for finding the orthogonal bases, we chose POD/SVD due to its significant model-space compression capability (Castleman, 1996). Figure 1 shows the first 20 principal basis vectors obtained from the 3000 TIs. As noted by Oware et al. (2018), the ranges of the sampling coefficients are critical to reconstructing physically realistic solute plumes. Hence, parameter bounds must be imposed on the resampling (equation 2) of the coefficients. To obtain physics-based parameter bounds for the prior coefficients, we map the TIs onto  $\mathbf{B}$ ; i.e.,

$$\mathbf{c}_{\text{prior}} = \mathbf{B}^T \mathbf{T}_i, \quad (4)$$

where  $\mathbf{T}_i$  is the set of TIs. There is a unique set of coefficients associated with each TI from the mapping in equation 4. Histogram analyses (not shown) of the 3000 coefficients associated with each coefficient reveal that most of the coefficients have approximately Gaussian distributions (e.g., Oware et al., 2018), which justifies an assumption of prior Gaussian distribution for the coefficients. Note that we also tested the assumption of prior uniform distribution over the range of each prior coefficient, but we found the prior Gaussian distribution to be superior.

We also inverted all the data sets using the classical smoothness-constrained inversion (SCI). We used the 2.5D ERT inversion code CRTomo (Kemna, 2000) for all resistivity forward simulations and the SCI. We used the following petrophysical relationship to convert the ERT tomograms into thermograms (e.g., Hermans et al., 2015):

$$T = \frac{1}{m_f} \left[ \frac{\sigma_T}{\sigma_b} \frac{\sigma_{fb}}{\sigma_{f,25}} - 1 \right] + 25, \quad (5)$$

where  $\sigma_b$  and  $\sigma_T$  are the inverted bulk electrical conductivity of the background and the time step of interest, respectively,  $\sigma_{fb}$  and  $\sigma_{f,25}$  denote, respectively, the fluid conductivity of the background and at a reference temperature (25°C), and  $m_f$  represents the fractional change in electrical conductivity per degree Celsius. The parameters  $\sigma_{f,25}$ ,  $\sigma_{fb}$ , and  $m_f$  were, respectively, set to 0.0791 S/m, 0.061 S/m, and  $0.0194^\circ\text{C}^{-1}$  (from Hermans et al., 2015).

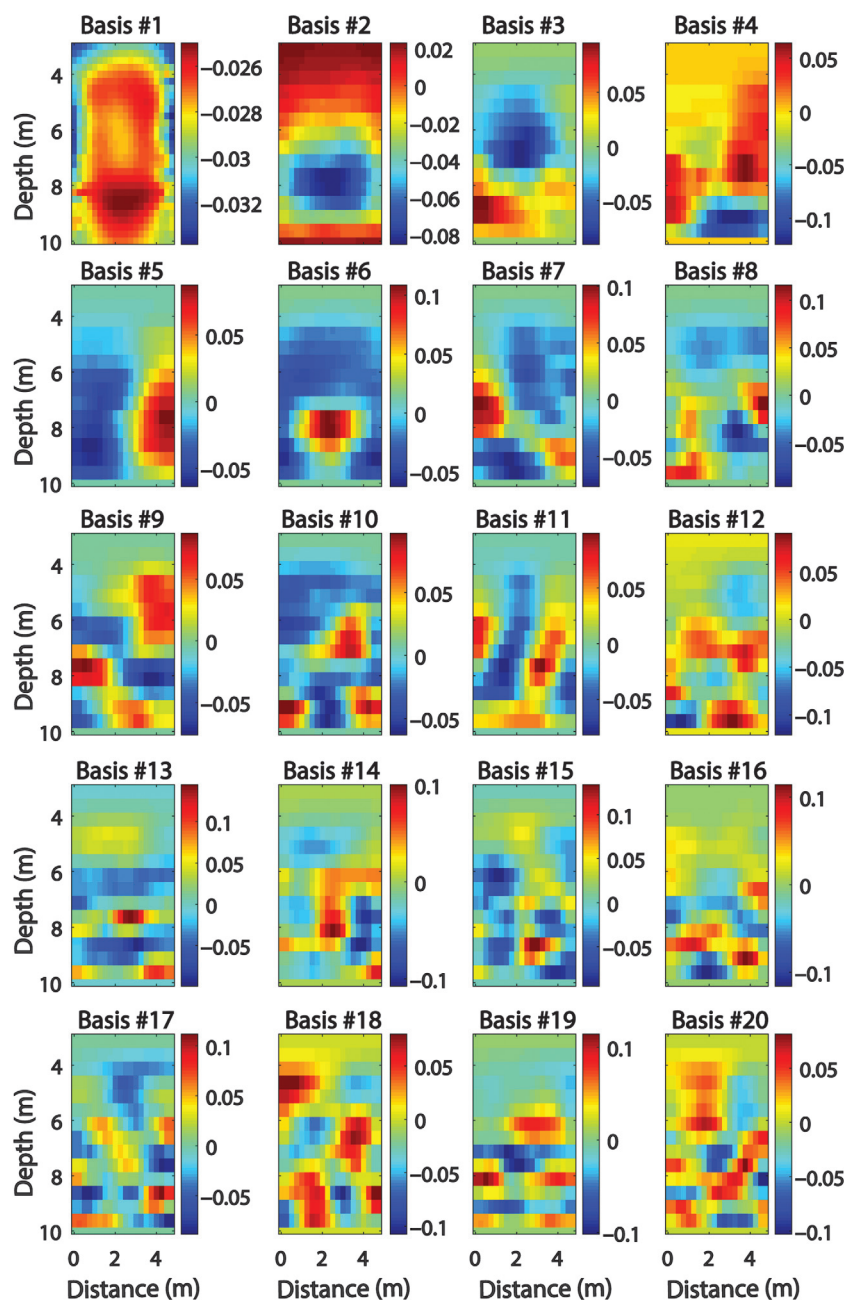


Figure 1. First 20 principal POD basis (POD heat plumes) constructed from the TIs. Note, the colorbars are not on the same scale because of loss of patterns in the bases with small values. The focus is on the patterns captured in each basis because the magnitudes will be scaled by the coefficients during the inversion.

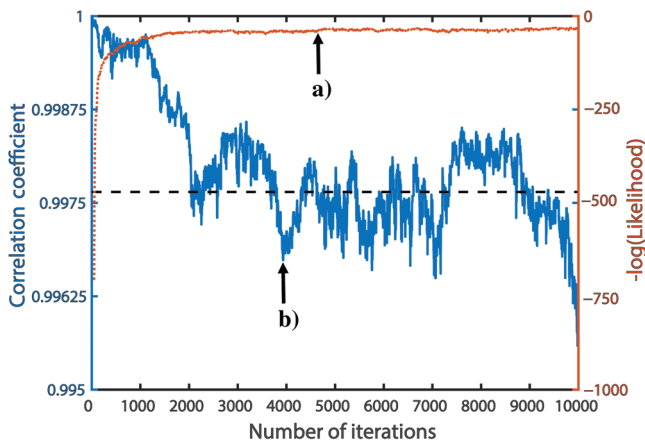


Figure 2. Sampling paths of (a) negative log-likelihood to determine the burn-in period and (b) correlation coefficient for autocorrelation analysis.

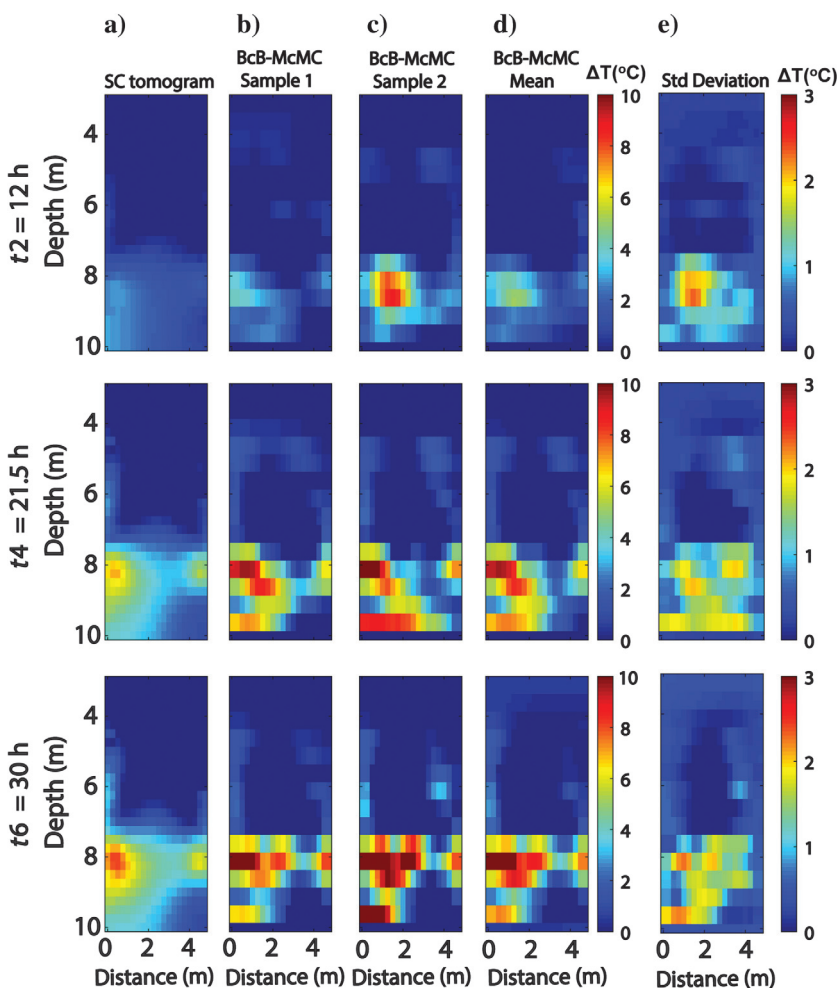


Figure 3. Difference thermograms recovered from the ERT measurements at three different time-steps: (row 1) 12 h, (row 2) 21.5 h, and (row 3) 30 h. Column (a) shows tomograms from the classic SCI, columns (b–e) show, respectively, two posterior realizations, posterior mean and standard deviations from the BC Bayesian Markov chain Monte Carlo difference inversion. The pz14 and pz15 are, respectively, located at (1.125, 9 m) and (2.25, 8.5 m).

## RESULTS AND DISCUSSION

We ran the algorithm for 120,000 iterations using 20 basis vectors (Figure 1) to reconstruct the 1092 full-dimensional space, resulting in more than 98% truncation in the dimensionality of the problem. The sampling path of the negative log-likelihood (equation 3, Figure 2a) shows rapid burn-in of the algorithm, with burn-in occurring at approximately 2000 iterations. We noted all the inversions burned in before the 4000 iteration mark. Hence, burn-in was set to 4000, resulting in a total of 116,000 posterior samples for all inversions. The rapid burn-in is attributable to the performance of the inversion in the reduced dimensional space. For instance, consideration of only 20 inversion parameters will reduce the search space significantly compared with sampling in the full dimensional pixel-based model space. Further, although all 20 coefficients can be perturbed at each iteration, it is impractical to do the same for all the model parameters of the full-dimensional space.

We performed model autocorrelation analysis to determine the number of iterations required to generate statistically independent samples (Figure 2b). The autocorrelation curve intercepts the average correlation level (the dashed line) at approximately 2000 iterations, which marks the correlation length. We repeated the analysis for multiple samples and found the correlation length to occur generally between iterations 2000 and 4000. We, therefore, set the correlation length to 3500 iterations, resulting in a total of 34 statistically independent posterior samples.

The difference thermograms recovered from the 12 ( $t_2$ ), 21.5 ( $t_4$ ), and 30 h ( $t_6$ ) time-steps based on the classical SCI and our approach are presented in Figure 3. Both strategies estimated similar locations and spatial extents of the heat plumes (Figure 3a–3d). Although smoothing of the heat plume is apparent in the SC tomograms (Figure 3a), our approach produced plume morphologies without excessive smoothing (Figure 3b–3d). This is ascribable to the incorporation of physics-based prior information in our approach. The standard deviation panels (Figure 3e) reveal the variabilities in uncertainty in the estimates. As expected, they show generally low uncertainty near the ERT well locations, a region of high data sensitivity. The ability of our strategy to reconstruct the different morphologies of the heat plume using the same set of basis constraints (BC) (Figure 1) illustrates the flexibility of the strategy to recombine the bases in a manner that honors the ERT measurements.

The validation of the estimated temperature breakthrough curves at the two piezometers, pz14 and pz15, is presented in Figure 4. Both strategies accurately predicted the general temporal behavior of the heat migration, with SCI out performing or underperforming our strategy at certain time steps. The 90% confidence interval (CI) of the estimates from our approach captured almost all of the true temperature measurements. In the data presented, a change of 1°C produced a

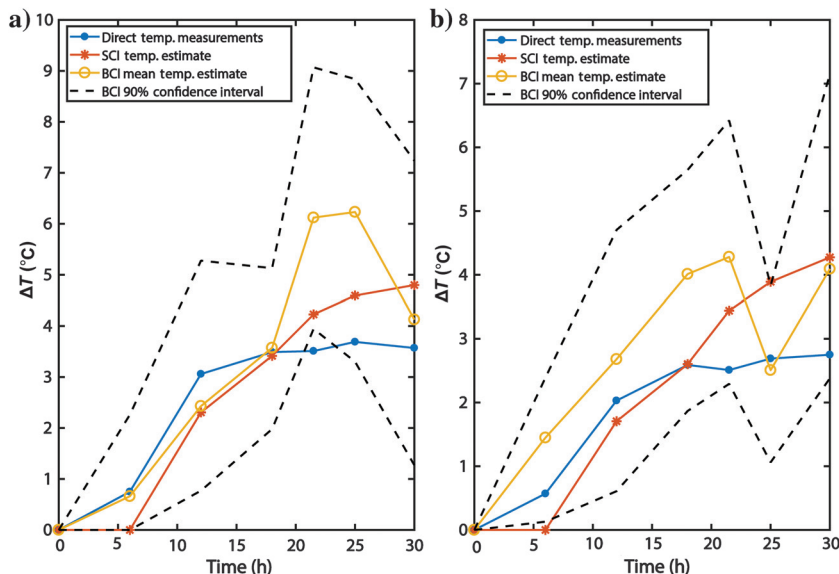


Figure 4. Validation of estimated temperature breakthrough curves at two validation locations: (a) pz14 and (b) pz15. (Blue lines) direct temperature measurements, and estimated temperature breakthrough curves from the (orange lines) classic SCI, (yellow lines) posterior mean of the BC Bayesian Markov chain Monte Carlo inversion. The two black dashed lines define the 90% CI of the BC estimates.

2% change in electrical conductivity (Hermans et al., 2018), which is undetectable in deterministic inversions. Hermans et al. (2015) estimate the limit of detection of ERT of this experiment at approximately 1.5°C. It appears that accounting for the physics of the target process improves the limit of detection in our approach. Specifically, 6 h ( $t_1$ ) of heat injection produced a change in temperature of approximately 0.5°C at pz14 and pz15 (Figure 4a and 4b). This small change in temperature was undetected by the SCI because it is well below the approximately 1.5°C ERT detection limit. Our approach, in contrast, accurately estimated the small temperature change and captured the true values within 90% CI of the mean, indicating that accounting for the physics of the target process potentially helps to improve estimation in poor data-resolution environments.

## CONCLUSION

The use of geophysical imaging to noninvasively investigate hydrogeologic processes is well-proven. Although SI is preferred for comprehensive interpretation and uncertainty assessment of geophysical estimates, the standard McMC method can become computationally prohibitive and unable to estimate physically realistic plume morphologies. We proposed here a novel basis-constrained Bayesian-McMC difference inversion framework. The strategy uses hydrologic-process tuned nonparametric basis vectors to account for the physics of the target process in a classic difference inversion framework in the reduced dimensionality space. This results in rapid burn-in of the algorithm, meaning a small number of geophysical forward simulations prior to burn-in, which can translate into gains in computational costs of the SI algorithms. We found that incorporating physics-based prior information not only produces physically realistic solute plumes without smoothing, but it also helps to improve estimation in poor data-resolution environments. Further research is, however, needed to demonstrate the full potential of physics-based

regularization to improve estimation in poor data-sensitivity environments.

## ACKNOWLEDGMENTS

We would like to thank D. Draganov, J. Blanch, and two anonymous reviewers for their insightful comments and constructive suggestions.

## DATA AND MATERIALS AVAILABILITY

Data associated with this research are available and can be obtained by contacting the corresponding author.

## REFERENCES

- Castleman, K. R., 1996, Digital image processing: Prentice Hall Inc.
- Day-Lewis, F. D., Y. Chen, and K. Singha, 2007, Moment inference from tomograms: *Geophysical Research Letters*, **34**, L22404, doi: [10.1029/2007GL031621](https://doi.org/10.1029/2007GL031621).
- Hansen, P. C., and D. P. O'Leary, 1993, The use of the L-curve in the regularization of discrete ill-posed problems: *SIAM Journal of Scientific Computing*, **14**, 1487–1503, doi: [10.1137/0914086](https://doi.org/10.1137/0914086).
- Hastings, W., 1970, Monte Carlo sampling methods using Markov chains and their applications: *Biometrika*, **57**, 97–109, doi: [10.1093/biomet/57.1.97](https://doi.org/10.1093/biomet/57.1.97).
- Hermans, T., F. Nguyen, M. Klepikova, A. Dassargues, and J. Caers, 2018, Uncertainty quantification of medium-term heat storage from short-term geophysical experiments using Bayesian evidential learning: *Water Resources Research*, **54**, 2931–2948, doi: [10.1002/wrcr.v54.4](https://doi.org/10.1002/wrcr.v54.4).
- Hermans, T., E. K. Oware, and J. K. Caers, 2016, Direct prediction of spatially and temporally varying physical properties from time-lapse electrical resistance data: *Water Resources Research*, **52**, 7262–7283, doi: [10.1002/2016WR019126](https://doi.org/10.1002/2016WR019126).
- Hermans, T., S. Wildemeersch, P. Jamin, P. Orban, S. Brouyere, A. Dassargues, and F. Nguyen, 2015, Quantitative temperature monitoring of a heat tracing experiment using cross borehole ERT: *Geothermics*, **53**, 14–26, doi: [10.1016/j.geothermics.2014.03.013](https://doi.org/10.1016/j.geothermics.2014.03.013).
- Hinnell, A., T. Ferré, J. Vrugt, J. Huisman, S. Moyssey, J. Rings, and M. Kowalsky, 2010, Improved extraction of hydrologic information from geophysical data through coupled hydrogeophysical inversion: *Water Resources Research*, **46**, W00D40, doi: [10.1029/2008WR007060](https://doi.org/10.1029/2008WR007060).
- Irving, J., and K. Singha, 2010, Stochastic inversion of tracer test and electrical geophysical data to estimate hydraulic conductivities: *Water Resources Research*, **46**, W11514, doi: [10.1029/2009WR008340](https://doi.org/10.1029/2009WR008340).
- Kemna, A., 2000, Tomographic inversion of complex resistivity: Theory and application: Ph.D. thesis, Bochum Ruhr University.
- LaBrecque, D. J., and X. Yang, 2001, Difference inversion of ERT data: A fast inversion method for 3-D in-situ monitoring: *Journal of Environmental and Engineering Geophysics*, **6**, 83–89, doi: [10.4133/JEEG6.2.83](https://doi.org/10.4133/JEEG6.2.83).
- Laloy, E., N. Linde, and J. A. Vrugt, 2012, Mass conservative three-dimensional water tracer distribution from Markov chain Monte Carlo inversion of time-lapse ground-penetrating radar data: *Water Resources Research*, **48**, W07510, doi: [10.1029/2011WR011238](https://doi.org/10.1029/2011WR011238).
- LeBlanc, D. R., S. P. Garabedian, K. M. Hess, L. W. Gelhar, R. D. Quadri, K. G. Stollenwerk, and W. W. Wood, 1991, Large-scale natural gradient tracer test in sand and gravel, cape cod, Massachusetts: 1. Experimental design and observed tracer movement: *Water Resources Research*, **27**, 895–910, doi: [10.1029/91WR00241](https://doi.org/10.1029/91WR00241).
- Linde, N., A. Binley, A. Tryggvason, L. B. Pedersen, and A. Revil, 2006, Improved hydrogeophysical characterization using joint inversion of cross-hole electrical resistance and ground-penetrating radar traveltime data: *Water Resources Research*, **42**, W12404, doi: [10.1029/2006WR005131](https://doi.org/10.1029/2006WR005131).
- Lochbuhler, T., S. J. Breen, R. L. Detwiler, J. A. Vrugt, and N. Linde, 2014, Probabilistic electrical resistivity tomography of a CO<sub>2</sub> sequestration analog: *Journal of Applied Geophysics*, **107**, 80–92, doi: [10.1016/j.jappgeo.2014.05.013](https://doi.org/10.1016/j.jappgeo.2014.05.013).
- MacKay, D. J. C., 1992, Bayesian interpolation: *Neural Computation*, **4**, 415–447, doi: [10.1162/neco.1992.4.3.415](https://doi.org/10.1162/neco.1992.4.3.415).
- Menke, W., 1984, Geophysical data analysis: Discrete inverse theory: Academic Press, 289.

- Metropolis, N., A. Rosenbluth, M. Rosenbluth, A. Teller, and E. Teller, 1953, Equation of state calculations by fast computing machines: *Journal of Chemical Physics*, **21**, 1087–1092, doi: [10.1063/1.1699114](https://doi.org/10.1063/1.1699114).
- Oware, E. K., 2016, Estimation of hydraulic conductivities using higher-order MRF-based stochastic joint inversion of hydrogeophysical measurements: *The Leading Edge*, **35**, 776–785, doi: [10.1190/le35090776.1](https://doi.org/10.1190/le35090776.1).
- Oware, E. K., M. Awatey, T. Hermans, and J. Irving, 2018, Basis-constrained Bayesian-McMC: Hydrologic process parameterization of stochastic geoelectrical imaging of solute plumes: 88th Annual International Meeting, SEG, Expanded Abstracts, 5472–5476, doi: [10.1190/segam2018-w12-01.1](https://doi.org/10.1190/segam2018-w12-01.1).
- Oware, E. K., and S. M. J. Moysey, 2014, Geophysical evaluation of solute plume spatial moments using an adaptive POD algorithm for electrical resistivity imaging: *Journal of Hydrology*, **517**, 471–480, doi: [10.1016/j.jhydrol.2014.05.054](https://doi.org/10.1016/j.jhydrol.2014.05.054).
- Oware, E. K., S. M. J. Moysey, and T. Khan, 2013, Physically based regularization of hydrogeophysical inverse problems for improved imaging of process-driven systems: *Water Resources Research*, **49**, 6238–6247, doi: [10.1002/wrcr.20462](https://doi.org/10.1002/wrcr.20462).
- Ruggeri, P., J. Irving, and K. Holliger, 2015, Systematic evaluation of sequential geostatistical resampling within MCMC for posterior sampling of near-surface geophysical inverse problems: *Geophysical Journal International*, **202**, 961–975, doi: [10.1093/gji/ggv196](https://doi.org/10.1093/gji/ggv196).
- Satija, A., and J. Caers, 2015, Direct forecasting of subsurface flow response from non-linear dynamic data by linear least-squares in canonical functional principal component space: *Advances in Water Research*, **77**, 69–81, doi: [10.1016/j.advwatres.2015.01.002](https://doi.org/10.1016/j.advwatres.2015.01.002).
- Singha, K., F. D. Day-Lewis, T. Johnson, and L. D. Slater, 2015, Advance in the interpretation of subsurface processes with time-lapse electrical imaging: *Hydrological Processes*, **29**, 1549–1576, doi: [10.1002/hyp.v29.6](https://doi.org/10.1002/hyp.v29.6).
- Tarantola, A., 2005, *Inverse problem theory and methods for model parameter estimation*: SIAM.
- Tikhonov, A. N., and V. Y. Arsenin, 1977, *Solutions of ill-posed problems*: John Wiley and Sons.